

Development of Potent Adenosine Monophosphate Activated Protein Kinase (AMPK) Activators

Eman M. E. Dokla,^[a, b] Chun-Sheng Fang,^[a] Po-Ting Lai,^[a] Samuel K. Kulp,^[a]
Rabah A. T. Serya,^[b] Nasser S. M. Ismail,^[b] Khaled A. M. Abouzid,^{*[b]} and Ching-Shih Chen^{*[a, c]}

Previously, we reported the identification of a thiazolidinedione-based adenosine monophosphate activated protein kinase (AMPK) activator, compound **1** (*N*-[4-({3-[(1-methylcyclohexyl)methyl]-2,4-dioxothiazolidin-5-ylidene)methyl}phenyl]-4-nitro-3-(trifluoromethyl)benzenesulfonamide), which provided a proof of concept to delineate the intricate role of AMPK in regulating oncogenic signaling pathways associated with cell proliferation and epithelial–mesenchymal transition (EMT) in cancer cells. In this study, we used **1** as a scaffold to conduct lead optimization, which generated a series of derivatives. Analysis of the antiproliferative and AMPK-activating activities of individual derivatives revealed a distinct structure–activity relationship and identified **59** (*N*-[3-nitrophenyl]-*N'*-{3-[(3,5-bis(trifluoromethyl)phenyl)methyl]-2,4-dioxothiazolidin-5-ylidene)methyl}phenyl)urea) as the optimal agent. Relative to **1**, compound **59** exhibits multifold higher potency in upregulating AMPK phosphorylation in various cell lines irrespective of their liver kinase B1 (LKB1) functional status, accompanied by parallel changes in the phosphorylation/expression levels of p70S6K, Akt, Foxo3a, and EMT-associated markers. Consistent with its predicted activity against tumors with activated Akt status, orally administered **59** was efficacious in suppressing the growth of phosphatase and tensin homologue (PTEN)-null PC-3 xenograft tumors in nude mice. Together, these findings suggest that **59** has clinical value in therapeutic strategies for PTEN-negative cancer and warrants continued investigation in this regard.

Introduction

Adenosine monophosphate activated protein kinase (AMPK) is a key player in maintaining energy homeostasis in response to metabolic stress.^[1–4] Beyond diabetes and metabolic syndrome,^[5] there is a growing interest in the therapeutic exploitation of the AMPK pathway in cancer treatment in light of its unique ability to regulate cancer cell proliferation through the reprogramming of cell metabolism.^[6–8] This premise was corroborated by the ability of the antidiabetic drug metformin, which acts by disrupting mitochondrial respiration, to activate AMPK, thereby lowering the risk of cancer and improving outcomes of many types of cancer cases.^[9,10] In addition to cell metabolism, recent evidence suggests that AMPK plays an intricate role in regulating cancer cell proliferation, survival, and invasive phenotype by targeting multiple oncogenic signaling pathways, including those mediated by Akt, mTOR, and

Introduction

MDM2.^[11–13] Consequently, the past few years have witnessed the development of a number of novel AMPK activators as discussed in several reviews,^[14–16] including A-769662,^[17] PT-1,^[18] OSU-53 (**1**; Figure 1),^[19] (*E*)-3-((3-[(4-chlorophenyl)(phenyl)methylene]-2-oxoindolin-1-yl)methyl)benzoic acid,^[20] and 991.^[14,21] Mechanistically, these direct activators circumvent the dependence on liver kinase B1 (LKB1), an upstream kinase of AMPK under conditions of energy stress, which is often inactivated in cancer cells through mutations in the course of tumorigenesis.^[13]

Previously, based on the screening of a thiazolidinedione-based focused compound library, we identified **1** as a direct AMPK activator in LKB1-deficient MDA-MB-231 cells.^[19] Compound **1** served as a proof-of-concept compound to delineate the intricate mechanisms by which AMPK regulates cell proliferation and epithelial–mesenchymal transition (EMT) in cancer cells,^[11,12] among which the ability of **1** to target the Akt–MDM2–Foxo3a signaling pathway is especially noteworthy. Specifically, pharmacological activation of AMPK leads to protein phosphatase 2A-facilitated Akt dephosphorylation. This Akt inactivation results in decreased phosphorylation of the E3 ligase murine double minute 2 (MDM2) and its substrate Foxo3a, which facilitates the cytoplasmic sequestration and nuclear translocation of MDM2 and Foxo3a, respectively. The physical separation of Foxo3a from MDM2 increases Foxo3a protein stability and accumulation.

These findings underscore the translational potential of targeting AMPK activation as a therapeutic strategy for metastatic

[a] E. M. E. Dokla, C.-S. Fang, P.-T. Lai, Dr. S. K. Kulp, Prof. C.-S. Chen
Division of Medicinal Chemistry & Pharmacognosy
College of Pharmacy, The Ohio State University
Room 336, Parks Hall, 500 West 12th Ave., Columbus, OH 43210 (USA)
E-mail: chen.844@osu.edu

[b] E. M. E. Dokla, Dr. R. A. T. Serya, Dr. N. S. M. Ismail, Prof. K. A. M. Abouzid
Pharmaceutical Chemistry Department, Faculty of Pharmacy
Ain Shams University, POB 11566, Abbassia, Cairo (Egypt)
E-mail: Khaled.abouzid@pharma.asu.edu.eg

[c] Prof. C.-S. Chen
Institute of Biological Chemistry, Academia Sinica
128 Academia Road Sec. 2, Nankang, Taipei (Taiwan)

Supporting information for this article is available on the WWW under
<http://dx.doi.org/10.1002/cmdc.201500371>.

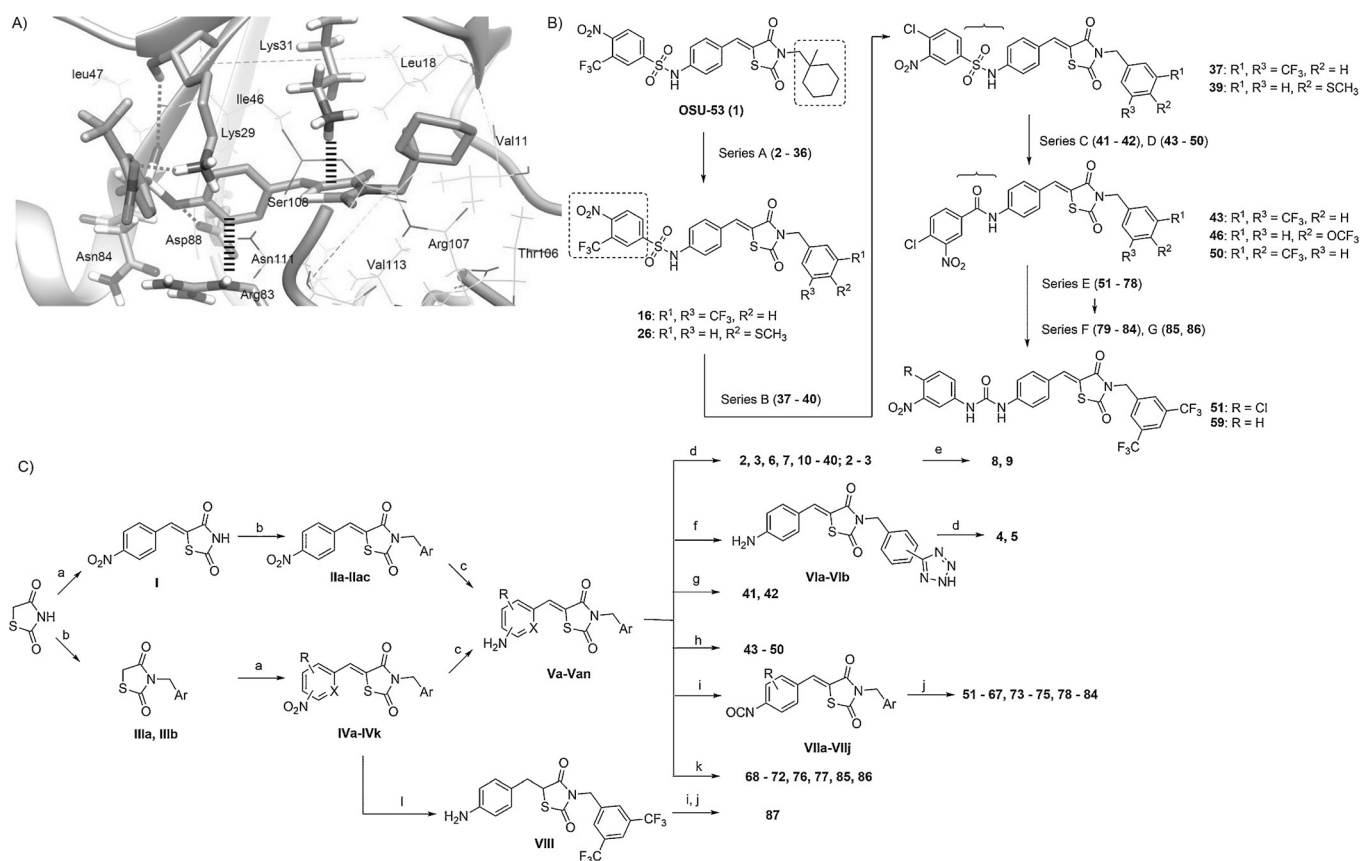


Figure 1. OSU-53 (1) as a scaffold to develop potent AMPK activators. A) Docking of 1 into the allosteric site formed at the interface between the kinase domain and CBM of AMPK (PDB ID: 4CFE). B) Schematic diagram depicting the strategies for lead optimization of compound 1. C) General synthetic procedures for compounds 2-87. *Reagents and conditions:* a) ArCHO, toluene, AcOH, piperidine, 80 °C, overnight; b) ArCH₂Br, MeCN, K₂CO₃, RT, 2 days; c) SnCl₂·2H₂O, EtOAc, reflux, 4-8 h; d) ArSO₂Cl, pyridine, RT, 3 days; e) derivatives 2 or 3, BH₃·DMS, THF, 70 °C, overnight; f) NaN₃, NH₄Cl, DMF, 125 °C, 24 h; g) morpholine carbonyl chloride, pyridine, RT, overnight; h) ArCOCl, pyridine, RT, overnight; i) phosgene, toluene, 100 °C, 2 h; j) ArNH₂, toluene, 100 °C, 12 h; k) ArNCS, DMF, RT, 12 h; l) 10% Pd/C, MeOH, 410 kPa, 16 h.

cancer treatment, thereby providing a rationale to use 1 as a scaffold to conduct lead optimization. This effort has netted a series of potent AMPK activators, among which 59 represented the optimal agent. Relative to 1, compound 59 was found to exhibit multifold higher potency in facilitating AMPK activation, accompanied by parallel changes in Akt phosphorylation and Foxo3a induction in MDA-MB-231 and other cancer cell lines. Equally important, 59 is orally active in suppressing xenograft tumor growth in nude mice without incurring acute toxicity.

Results

Structural optimization of 1

We carried out modeling analysis by docking 1 into the recently released X-ray crystal structure of human AMPK (PDB ID: 4CFE).^[22] This analysis revealed that 1 binds key amino acids in the allosteric site formed at the interface between the kinase domain and carbohydrate binding module (CBM) through the following forces, as depicted in Figure 1 A.

- Hydrophobic interactions between the cyclohexane/benzylidene moieties and the large hydrophobic pocket formed by residues Val11, Leu18, Ile46, and Leu47 (kinase domain) and Val81, Val113, and Val118 (CBM domain);
- Cation- π interactions between the thiazolidinedione ring and Lys31 (kinase domain), as well as between the benzylidene ring and Arg83 (CBM);
- Hydrogen bonding between the -SO₂NH- moiety and Lys29 and Asp88, and between the -NO₂ substituent and Lys29.

Based on this docking analysis, we used the following strategies to conduct the structural modification of 1 (Figure 1 B). General procedures for the synthesis of these compounds are depicted in Figure 1 C. The initial screening was based on the activities of individual compounds, each at 5 μ M, in suppressing the viability of LKB1-deficient MDA-MB-231 cells by using MTT assays.

Step 1 (Series A): The methylcyclohexyl group of 1 was replaced with various substituted phenyl rings to exploit the hydrophobic pocket. Among 35 derivatives (2-36) examined (Figure 2), 16 [3,5-di(trifluoromethyl)phenyl] and 26 [4-(methylthio)phenyl] exhibited moderately higher antiproliferative potencies than compound 1 (Figure 3 A).

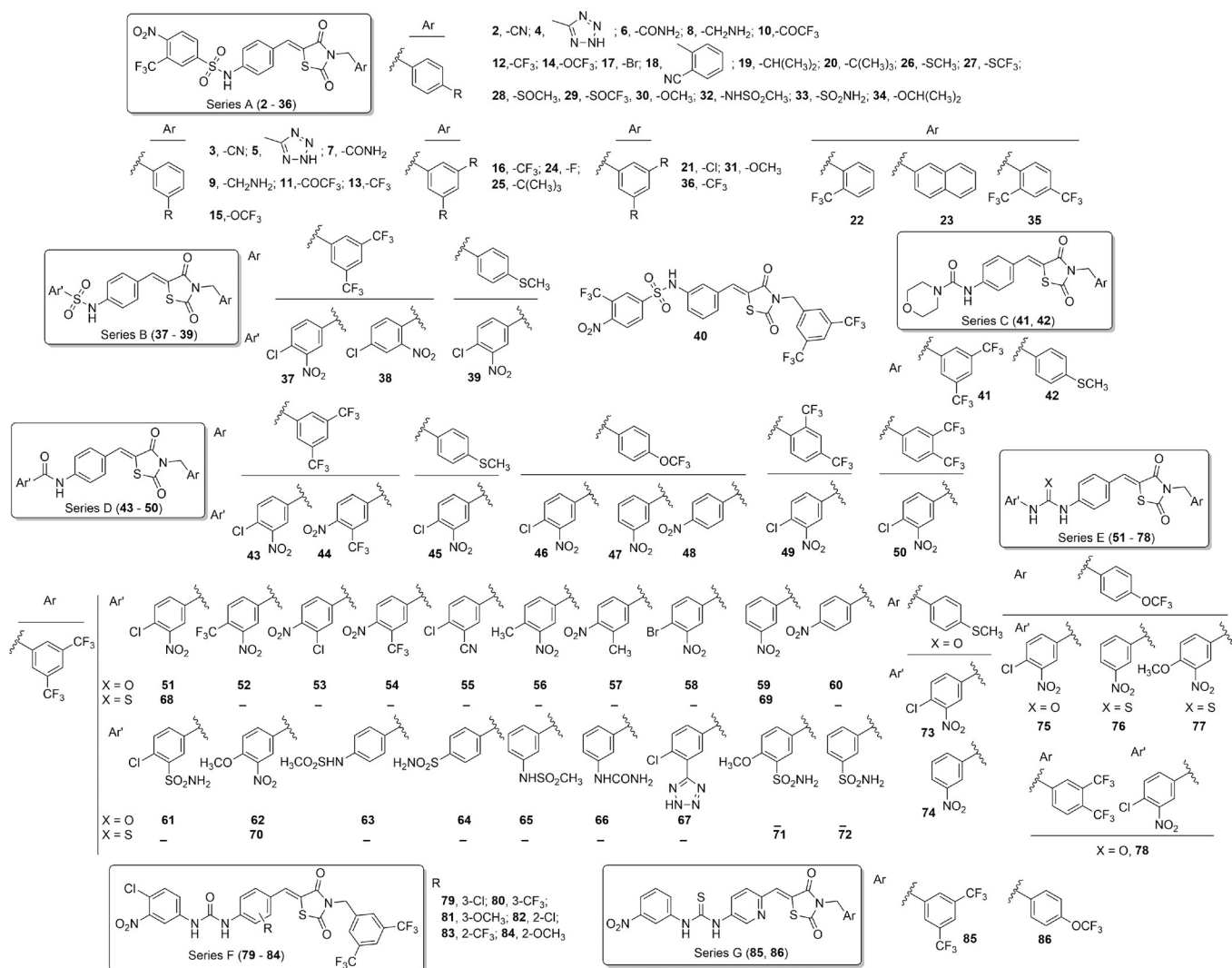


Figure 2. Structures of compounds 2–86 in Series A–G.

Step 2 (Series B): The 3-trifluoromethyl-4-nitrophenyl ring of **16** and **26** were replaced with 4-chloro-3-nitro- or 4-chloro-2-nitrophenyl moieties to generate compounds **37–39** (Figure 2). As shown, substitution of the 3-trifluoromethyl-4-nitrophenyl moiety of **16** and **26** with 4-chloro-3-nitro- substantially increased the antiproliferative activities of the resulting compounds (**37** and **39**; Figure 3A). Relative to **37**, the antiproliferative potency of **38** was attenuated as a result of the different configuration of the nitro group on the phenyl ring, indicating its distinct role in interacting with the binding motif. Moreover, **40**, a regioisomer of **16**, was synthesized and assessed for its *in vitro* antiproliferative activity, which was abolished by the change in the regiochemical configuration of the terminal phenylsulfonamide substructure.

Step 3 (Series C–E): As bioisosteric replacement represents a common strategy for lead optimization,^[23,24] we tested the effects on antiproliferative efficacy of replacing the sulfonamide linker with amide (Series C, **41** and **42**; Series D, **43–50**), urea (Series E, **51–67**, **73–75**, and **78**), and thiourea (Series E,

68–72, **76**, and **77**) in conjunction with varying the terminal substituted phenyl moiety (Figure 2). This strategy generated an array of derivatives with the ability to suppress cell viability by $\geq 75\%$ at $5 \mu\text{M}$, which included **43**, **46–48**, **50–54**, **59**, **62**, **68**, **69**, **71**, **74**, and **75** (Figure 3A). A unique feature common to many of these compounds is the 3-nitrophenyl moiety, with the exception of **71**, in which the 3-nitro substituent was replaced by a sulfonamide function.

Step 4 (Series F and G): Continued structural modifications of the two optimal derivatives **51** and **59** generated Series F (**79–84**) and G (**85**, **86**), respectively (Figure 2). Substitution on the benzylidene moiety of **51** with various functionalities, including chloro, trifluoromethyl, and methoxy, at the C2' and, to a great extent, C3' positions diminished antiproliferative efficacy relative to the parent compound (Figure 3A), indicating the distinct stereoelectronic effect of these substituents. In particular, the addition of a chlorine atom to the C2' position completely abolished activity. Replacement of the phenyl ring of the benzylidene moiety of **59** with a pyridine and/or replacing the ter-

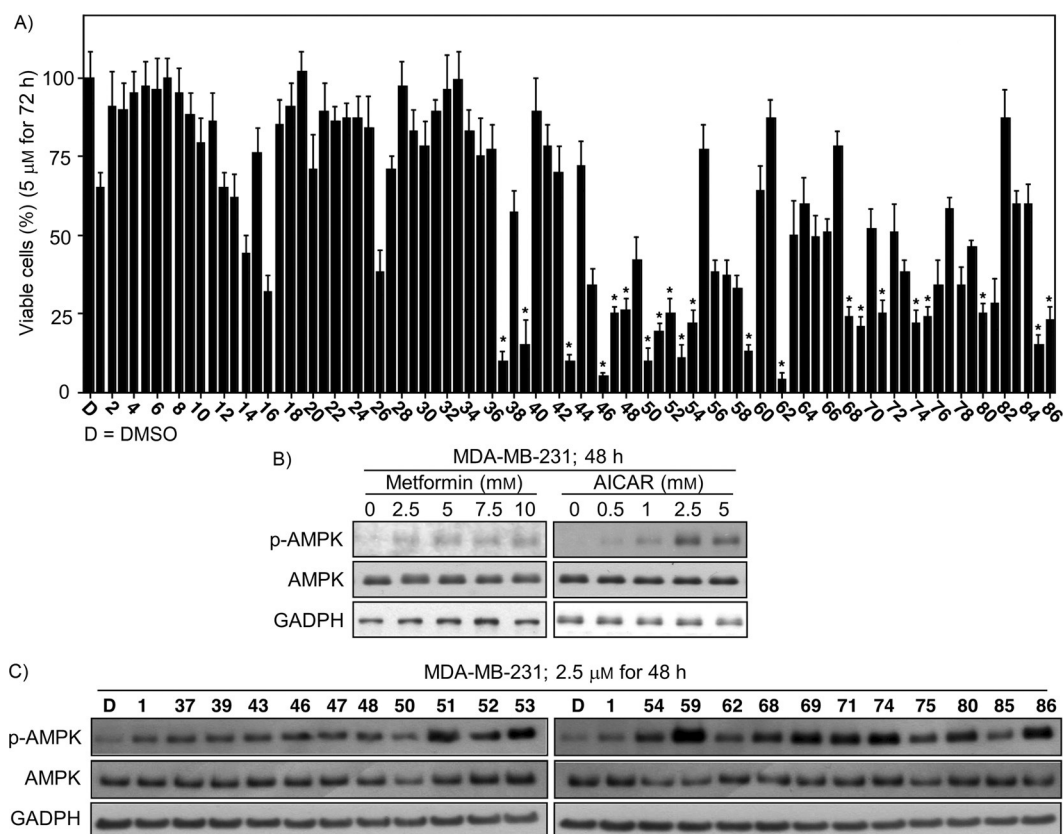


Figure 3. Identification of optimal AMPK activators. A) Effects of **1–86**, each at 5 μM , relative to DMSO control on the viability of MDA-MB-231 cells after 72 h of incubation by MTT assays; data are the mean \pm SD ($n=6$); *compounds with the ability to suppress $\geq 75\%$ cell viability. Western blot analysis of B) dose-dependent effects of metformin (left) and AICAR (right), and C) effects of selected derivatives, each at 2.5 μM , on AMPK phosphorylation in MDA-MB-231 cells after 48 h of treatment.

minal 3,5-di(trifluoromethyl)phenyl with 4-trifluoromethylphenyl (**85** and **86**, respectively) did not show improved potency relative to **59**.

Identification of optimal AMPK activators by cell-based assays

Of the 85 derivatives examined, 21 compounds were found to be effective in suppressing the viability of MDA-MB-231 cells by $\geq 75\%$ at 5 μM after 72 h of exposure, including **37**, **39**, **43**, **46–48**, **50–54**, **59**, **62**, **68**, **69**, **71**, **74**, **75**, **80**, **85**, and **86** (Figure 3A, indicated by *). We further assessed the effects of these compounds vis-à-vis **1** on the phosphorylation status of AMPK in MDA-MB-231 cells by western blot analysis. Due to a lack of LKB1, MDA-MB-231 cells were resistant to the effect of metformin-induced metabolic stress on AMPK activation (Figure 3B, left), reminiscent to that previously reported.^[25] In addition, these cells were relatively insensitive to 5-aminoimidazole-4-carboxamide ribonucleotide (AICAR)-facilitated AMPK phosphorylation (right). In contrast, these derivatives exhibited differential effects on AMPK phosphorylation, with **59** showing the highest potency, among those with high activity, including **51**, **53**, **69**, **71**, **74**, and **86** (Figure 3C). Based on these data, **59**,

its close derivative **51**, and **71** were selected for further evaluations vis-à-vis compound **1**.

MTT assays revealed a positive correlation between the anti-proliferative efficacies of these compounds (IC_{50} values at 72 h: **59**, 1.8 μM ; **51**, 3.5 μM ; **71**, 4 μM ; **1**, 6 μM ; Figure 4A) and their aforementioned abilities to upregulate AMPK phosphorylation (Figure 3C). This observation was confirmed by the differences in their dose-dependent effects on AMPK phosphorylation, which was accompanied by parallel increases in the phosphorylation of its downstream substrate acetyl-CoA carboxylase (ACC; Figure 4B). Whereas **59** was effective in inducing AMPK phosphorylation at ≤ 1 μM , other compounds examined would require substantially higher concentrations (**1**, 7.5 μM ; **51**, 2.5 μM ; **71**, 2.5–5 μM) to achieve the same level of increase in AMPK phosphorylation.

Mechanistic interrogation of the effects of **51**, **59**, and **71** on AMPK signaling

It is well recognized that AMPK acts as an energy sensor by mediating the phosphorylating inactivation of ACC and other key lipogenic enzymes in response to cellular AMP or ADP elevation.^[1] Equally important, we previously used **1** as a proof-of-concept compound to demonstrate the suppressive effect of

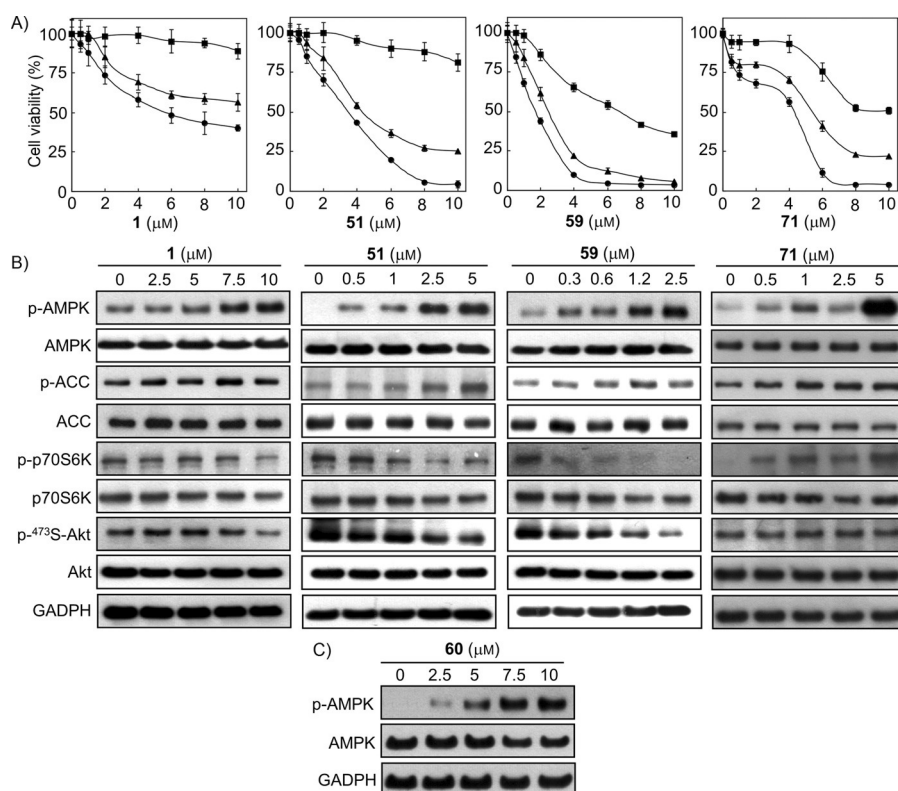


Figure 4. A) Time [24 (■), 48 (▲), and 72 h (●)] and dose-dependent suppressive effects of **51**, **59**, and **71** versus **1** on the viability of MDA-MB-231 cells as determined by MTT assays. Data are the mean \pm SD ($n=6$). B) Western blot analysis of the dose-dependent effects of individual agents on the phosphorylation of AMPK and downstream targets, including ACC, p70S6K, and Akt in MDA-MB-231 cells after 48 h of exposure. C) Dose-dependent effects of **60** on the phosphorylation of AMPK in MDA-MB-231 cells after 48 h of exposure.

AMPK activation on multiple oncogenic signaling pathways, including those mediated by Akt and mTOR/p70S6K.^[11,12] Consequently, as part of the mechanistic interrogation of **59**, **51**, and **71**, we compared their effects versus those of **1** on these aforementioned signaling markers. As shown, **59** (0.3–2.5 μM) and, to a slightly lesser extent, **51** (0.5–5 μM) were effective in increasing the phosphorylation of AMPK and its target ACC, accompanied by parallel decreases in the phosphorylation of p70S6K, a marker of mTOR activity, and Akt in a manner reminiscent of that of **1** (2.5–10 μM) in MDA-MB-231 cells (Figure 4B). In contrast, **71**, unlike **59** and **51**, was ineffective in downregulating the phosphorylation of p70S6K and Akt, suggesting a clear structure–activity relationship (SAR) among these three AMPK-activating agents in modulating AMPK downstream effectors (see the following section for further discussion). This distinct SAR was further manifested by **60**, which differs from **59** in the substitution position of the nitro group (C4 versus C3). Despite largely shared structural motifs, **60** exhibited substantially lower efficacy than **59** in suppressing viability (IC_{50} : 6 μM versus 1.8 μM for **59**, data not shown) and eliciting AMPK activation (Figure 4C) in MDA-MB-231 cells.

To refute the possibility that the capacity of **59** to activate AMPK signaling is unique to MDA-MB-231 cells, we expanded our investigation to two additional cell lines, MDA-MB-468 breast cancer cells and phosphatase and tensin homologue

(PTEN)-null PC-3 prostate cancer cells. MTT assays indicate that the antiproliferative efficacies of **1** and **59** in MDA-MB-468 and PC-3 cells are similar to those in MDA-MB-231 cells with the respective IC_{50} values as follows: **1**, 5.8 and 6.2 μM; **59**, 1.5 and 1.6 μM (data not shown). More important, **1** and **59** affected AMPK phosphorylation and various AMPK downstream markers in these two cell lines in a manner similar to that in MDA-MB-231 cells (Figure 5A,B), indicating these effects are not a cell-line-specific phenomenon. Moreover, consistent with our previous results demonstrating the role of AMPK in suppressing EMT via Foxo3a upregulation,^[12] exposure of MDA-MB-231 and PC-3 cells to **59** dose-dependently increased Foxo3a expression, leading to the reversal of their mesenchymal phenotype, as manifested by increases in the epithelial markers claudin-1 in MDA-MB-231 cells, which are deficient in E-cadherin, and E-cadherin in PC-3 cells, in conjunction with parallel decreases

in the mesenchymal markers vimentin and snail in both cell lines (Figure 5C).

59 is not a PAINS compound

It has recently been reported that so-called pan-assay interference (PAINS) compounds—those with certain classes of chemically reactive substructures—could give rise to false-positive results by interfering with assays through covalent modifications, metal chelation, photometric interference, redox activity, and/or aggregate formation.^[26–28] These types of interference might lead to false leads that could not be optimized. Families of these PAINS compounds include alkyldiene-containing heterocycles, hydroquinones, catechols, hydroxyphenylhydrozones, Mannich bases of phenols, and 2-amino-3-carbonyl thiophenes. Although **59** was not recognized by the PAINS filters (<http://cbligand.org/PAINS/login.php>),^[27] it contains an alkyldiene thiazolidinedione substructure, which could serve as a Michael acceptor to covalently modify the target protein AMPK upon binding. This possibility was refuted by the distinct SAR displayed by various close derivatives of **59** in activating AMPK, as demonstrated in Figures 3 and 4. Moreover, we obtained two additional lines of evidence to support the position that **59** is not a PAINS compound. First, compound **87**, a saturated counterpart of compound **59**, retained the ability to sup-

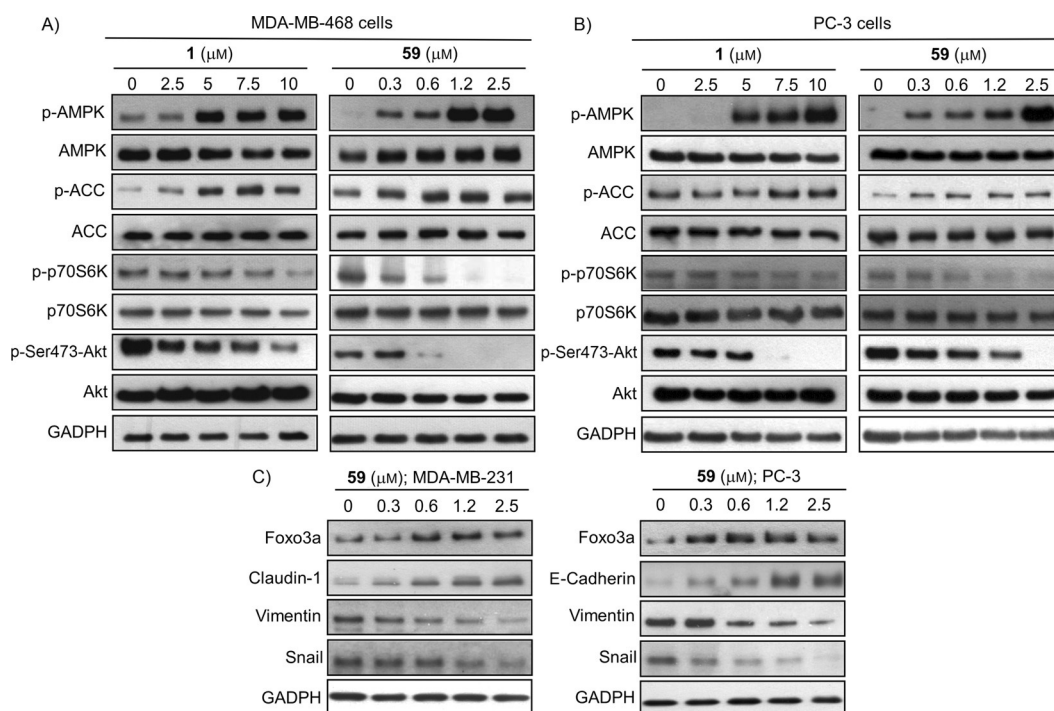


Figure 5. Western blot analysis of the effect of compound **59** versus **1** on the phosphorylation of AMPK, ACC, p70S6K, and Akt in A) MDA-MB-468 and B) PC-3 cells after 48 h of treatment. C) Suppressive effect of **59** on EMT in MDA-MB-231 and PC-3 cells, as manifested by increases in the expression of Foxo3a and the epithelial marker claudin-1 or E-cadherin, accompanied by parallel decreases in the expression of the mesenchymal markers vimentin and snail.

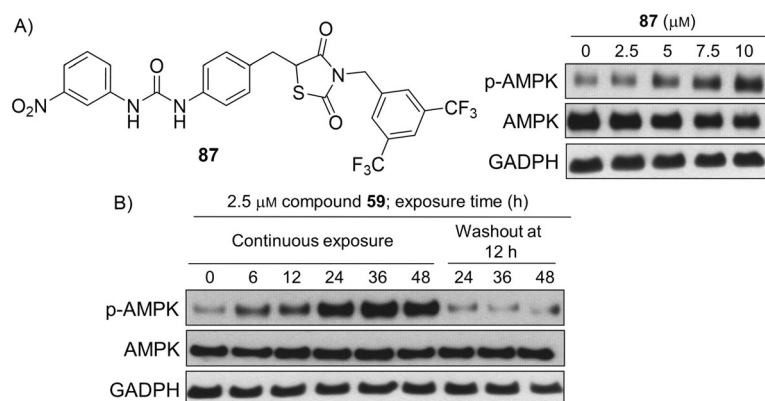


Figure 6. Evidence that **59** is not a PAINS compound. A) Structure of **87**, a saturated derivative of **59** (left); western blot analysis of the dose-dependent effects of **87** on the phosphorylation of AMPK in MDA-MB-231 cells after 48 h of exposure (right). B) Time-dependent effects of **59**, via continuous exposure or removal (washout) after 12 h of drug exposure, on the phosphorylation of AMPK in MDA-MB-231 cells.

press cell viability (IC_{50} : 9 μM, data not shown) and to activate AMPK, although with lower potency, in MDA-MB-231 cells (Figure 6A).

The lower efficacy of **87** in eliciting AMPK activation might arise from loss of the rigid conformation associated with the removal of the double bond, resulting in weaker interactions with the binding motif. Second, we conducted a washout experiment, in which **59** was removed from the culture medium after 12 h of drug exposure. In principle, if the mode of AMPK activation by **59** was mediated through the formation of covalent

adducts, the course of enzyme activation would not be adversely affected by drug removal. However, this washout experiment indicated that AMPK phosphorylation in drug-treated MDA-MB-231 cells returned to the basal level following the removal of **59** from the medium (Figure 6B). This rapid restoration of AMPK phosphorylation suggests a reversible nature of this ligand–protein interaction.

In vivo efficacy of **59** versus **1** in suppressing PC-3 xenograft tumor growth

Based on the above findings, we selected **59** as the lead AMPK activator vis-à-vis **1** for the evaluation of in vivo efficacy. In light of the ability of **59** to target the AMPK–Akt signaling axis, we examined **59** versus **1** as a single agent against the growth of subcutaneous xenograft tumors established from PTEN-null PC-3 cells in athymic nude mice ($n=7$ for each group). As shown, daily administration of **59** at 50 mg kg⁻¹ via oral gavage significantly suppressed PC-3 xenograft tumor growth after 28 days of treatment (65% inhibition, $p=0.0003$ relative to vehicle-treated control; Figure 7A, left).

In contrast, **1** gave rise to modest, but statistically insignificant inhibition (36% inhibition; $p=0.069$). Equally important, **59** was well tolerated, as no significant loss of body weight was noted (Figure 7A, right). Moreover, western blot analysis of tumor lysates showed that this tumor-suppressive activity correlated with the ability of **59** to activate AMPK signaling, as manifested by parallel changes in the phosphorylation levels

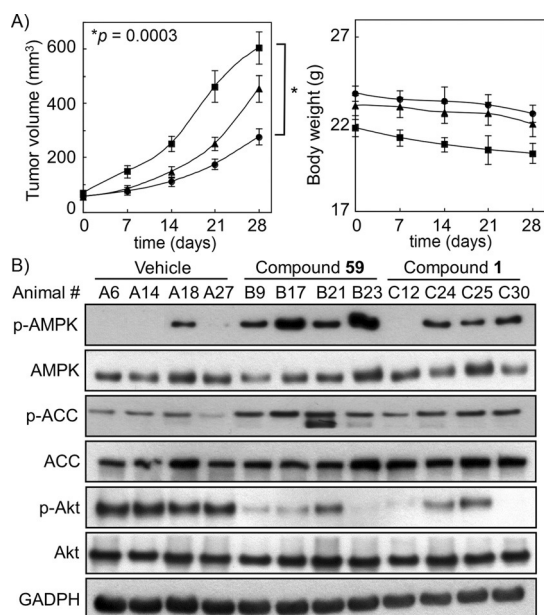


Figure 7. A) In vivo efficacy of **59** (●) versus **1** (▲) in suppressing PC-3 xenograft tumor growth; vehicle control (■) is shown for comparison. Athymic nude mice bearing established subcutaneous PC-3 xenograft tumors were treated once daily with vehicle, **1**, or **59** via oral gavage at 50 mg kg⁻¹ for 28 days. Tumor volume (left) and body weight (right) data are presented as means ± SEM (*n* = 7). B) Western blot analysis of the phosphorylation of AMPK, ACC, and Akt in lysates from four representative tumors from each group of mice after 28 days of treatment.

of AMPK, ACC, and Akt (Figure 7B). As compared with **1**, compound **59** elicited a greater extent of AMPK activation in tumors.

Discussion

Using **1** as a proof of concept, we previously demonstrated the relevance of AMPK activation as a therapeutic strategy to suppress tumorigenesis and invasive phenotype by targeting multiple oncogenic pathways.^[11,12] However, **1** exhibited modest potency in facilitating AMPK activation, which underlies the impetus of lead optimization of **1** to develop more potent AMPK activators. Based on modeling analysis, we modified different substructures of compound **1** in a stepwise manner, as outlined in Figure 1B, to generate a total of 85 derivatives, among which **59** represented the lead agent. Analysis of the antiproliferative and/or AMPK-activating activities of individual derivatives revealed a distinct SAR. Among various functionalities that were modified, the linker between the two aromatic systems and the nitro substituent on the phenyl ring had the most profound effects on the aforementioned activities. Among the 21 derivatives selected for western blot analysis (Figure 3C), compounds with a urea linker (**51–54**, **59**, **62**, **68**, **69**, **71**, **74**, **80**, **85**, **86**) generally showed superior potency in facilitating AMPK phosphorylation relative to those containing sulfonamide (**37**, **39**) or amide (**43**, **46–48**, **50**) groups (Figure 3C). Moreover, shifting the orientation of the nitro function of **59** (C3→C4) substantially attenuated the antiproliferative and AMPK-activating activities of the resulting compound **60**.

This role of the nitro substituent in mediating AMPK activation was also manifested by the differential activity between **51** and **59**. Relative to **59**, compound **51** showed lower activities in antiproliferation and AMPK activation, which might be due to the stereochemical effect of the additional chlorine atom on protein binding. Together, these data suggest intricate interplay between the nitro substituent on the terminal phenyl ring and neighboring functionalities in interacting with the binding pocket of AMPK. Compound **59** exhibited multifold higher potency than **1** in upregulating the phosphorylation of AMPK and its downstream target ACC in multiple cell lines, irrespective of their LKB1 functional status. Equally important, this AMPK activation was accompanied by parallel changes in the phosphorylation/expression levels of p70S6K, Akt, Foxo3a, and various EMT-associated markers, confirming its ability to target the AMPK–Akt–Foxo3a signaling axis.

Our previous study demonstrated the in vivo efficacy of **1** in suppressing PTEN-functional MDA-MB-231 xenograft tumor growth.^[11] In light of its predicted activity against tumors with activated Akt status, we examined the tumor-suppressive activity of **59** versus **1** (50 mg kg⁻¹ daily via oral gavage) in PTEN-null PC-3 tumor-bearing athymic nude mice. Consistent with the relative in vitro antiproliferative potency, **59** showed higher in vivo efficacy than **1** in inhibiting PC-3 xenograft tumor growth, which correlated with their respective activities in facilitating AMPK activation in tumors. Together, these findings suggest that **59** has clinical value in therapeutic strategies for PTEN-negative cancer and warrants continued investigation in this regard.

PAINS have become a major issue in drug discovery because they give rise to false-positive results in enzyme-based assays due to their confounding properties, which would lead to problematically flat SAR if the chemically reactive substructure remains unchanged.^[26–28] In our study, there was a clear SAR in the course of optimization, and it is notable that disruption of the conjugated system by removing the double bond did not abrogate the ability of the resulting compound, i.e., **87**, to activate AMPK, although with lower potency. In addition, the washout experiment indicates the ligand–protein binding is reversible, which, in conjunction with the improved in vitro and in vivo antitumor efficacy of **59** relative to **1** by targeting the AMPK–Akt signaling axis, refutes the possibility that **59** behaves like a PAINS compound.

Conclusions

In light of the demonstrated ability of compound **1** to target the Akt–Foxo3a signaling pathway via AMPK activation, this study described the lead optimization of **1** to develop a series of potent AMPK activators. This effort netted the lead compound **59**, which displayed high in vitro and in vivo efficacy in activating AMPK and suppressing PTEN-negative tumor growth, which might have translational potential in fostering novel therapeutic strategies for cancer therapy.

Experimental Section

Chemistry

Detailed information on the syntheses of compounds **2–87** is given in the Supporting Information. Compound **1** was synthesized as previously reported (compound **53** therein).^[19] All commercially available reagents were used without further purification unless otherwise stated. Routine ¹H and ¹³C NMR spectra were recorded on Bruker AV300 or Bruker Ascend 400 instruments. Samples were dissolved in CDCl₃ or deuterated dimethyl sulfoxide ([D₆]DMSO), and tetramethylsilane (TMS) was used as a reference. Electrospray ionization mass spectrometry analyses were performed with a Micromass Q-ToF II high-resolution electrospray mass spectrometer at The Ohio State University Campus Chemical Instrument Center. All compounds used for bioassays were characterized by ¹H NMR, ¹³C NMR, and HRMS, and were found to have purity >95%. The purity of all compounds was confirmed by a Hitachi Elite LaChrom HPLC system (including a Versa Grad Prep 36 pump, an L-2400 UV detector, an L-2200 autosampler, and a 150×4.6 mm Agilent ZORBAX Eclipse XDB-C₁₈ 5μ column; detection: λ 360 nm). A linear solvent gradient with a mobile phase of 40% H₂O in CH₃CN to 100% CH₃CN in 30 min was used.

Docking analysis

Docking was performed with the Discovery Studio CDocker protocol (version 2.5, Accelrys Inc., San Diego, CA, USA). The X-ray crystal structure of human AMPK was obtained from the RCSB Protein Data Bank server (PDB ID: 4CFE). The protein structure was prepared according to the standard protein preparation procedure integrated in Accelrys Discovery Studio 2.5, which involved adding hydrogen atoms, completing the missing loops, and assigning force field parameters. CHARMM force field was used for simulation studies, and then the protein structure was minimized using 1000 iterations of steepest descent minimization algorithm. The ligands were drawn using the sketching tools of Accelrys Discovery Studio and were prepared for docking by adding hydrogen atoms and partial charges using the Momany–Rone method. The CDocker protocol was used for docking. The binding site was defined by the residues within 10 Å distance from the co-crystallized ligand. The default values of CDocker were used. Ten different docking solutions were generated and visually inspected for selection of the best binding mode. The docking mode was represented using Chimera software version 1.8.1.^[29]

Biological methods

Cell lines, culture, reagents, and antibodies: The MDA-MB-231 and MDA-MB-468 breast cancer and PC-3 prostate cancer cell lines were purchased from American Type Culture Collection (Manassas, VA, USA). Media used for the maintenance of these cells were as follows: MDA-MB-231 and MDA-MB-468, DMEM; PC-3, RPMI 1640, all of which were supplemented with 10% fetal bovine serum (FBS). Cells were incubated at 37 °C in a humidified incubator containing 5% CO₂. MTT [3-(4,5-dimethylthiazol-2-yl)-2,5-diphenyl-2H-tetrazolium bromide] was obtained from TCI America (Portland, OR, USA), and the ECL Western Blotting System was from GE Healthcare Life Sciences (Pittsburgh, PA, USA). Antibodies specific for the following protein targets were used: p-Thr172-AMPK, AMPK, p-Thr389-p70S6K, p70S6K, Ser473-Akt, Akt, Foxo3a, claudin-1, vimentin, snail, and β-actin (Cell Signaling Technology Inc., Beverly, MA, USA); E-cadherin, BD Biosciences (San Diego, CA, USA).

Alexa Fluor 555- and 488-conjugated goat anti-rabbit and anti-mouse IgG were purchased from Invitrogen (Carlsbad, CA, USA), and anti-mouse and anti-rabbit secondary antibodies were obtained from Jackson ImmunoResearch Laboratories (West Grove, PA, USA).

Cell viability assay: Cell viability was assessed by using the MTT assay in six replicates. Cells were seeded and incubated in 96-well plates in the respective medium with 10% FBS for 24 h, and then exposed to test agents at the indicated concentrations dissolved in DMSO in 5% FBS-supplemented medium. After 72 h of treatment, the medium was removed and replaced by 200 μL of 0.5 mg mL⁻¹ MTT in 10% FBS-containing medium, and cells were incubated at 37 °C for 2 h. Supernatants were removed, and the MTT dye was solubilized in DMSO (120 μL per well). Absorbance at λ 570 nm was determined on a plate reader. Cell viabilities are expressed as percentages of that in the corresponding vehicle-treated control group.

Cell lysis and immunoblotting: Cells were exposed to the test agents in 10 cm dishes and then collected by scraping. The cell pellets were washed once with PBS, and then lysed in SDS lysis buffer containing 50 mM Tris-HCl (pH 8), 10 mM EDTA, 1% SDS, and a commercial protease inhibitor cocktail (2 mM AEBSEF, 1 mM EDTA, 130 μM bestatin, 14 μM E-64, 1 μM leupeptin, 0.3 μM aprotinin). After centrifugation of lysates for 20 min at 14000×g, the supernatants were collected. A sample of each supernatant (1 μL) was used for determination of protein concentration using a colorimetric bicinchoninic acid assay (Pierce, Rockford, IL, USA), and to the remaining sample was added an equal volume of 2× SDS-PAGE sample loading buffer (62.5 mM Tris-HCl, pH 6.8, 4% SDS, 5% β-mercaptoethanol, 20% glycerol, 0.1% bromophenol blue), followed by incubation in boiling water for 5 min. Equivalent amounts of proteins were resolved by SDS-PAGE, and then transferred to nitrocellulose membranes using a semidry transfer cell. The transblotted membrane was washed twice with Tris-buffered saline containing 0.1% Tween 20 (TBST). After blocking with TBST containing 5% nonfat milk for 40 min, the membrane was incubated with the appropriate primary antibody (1:1000) in TBST-1% nonfat milk at 4 °C overnight. The membrane was then washed three times with TBST for a total of 15 min, followed by incubation with goat anti-rabbit or anti-mouse IgG-horseradish peroxidase conjugates (1:2000) for 1 h at room temperature and four washes with TBST for a total of 1 h. The immunoblots were visualized by enhanced chemiluminescence.

Testing the in vivo efficacy of **1 and **59** in PC-3 tumor-bearing nude mice:** Athymic nude mice (Hsd:ATHYMIC Nude-Foxn1tm; 5–6 weeks of age; Harlan, Indianapolis, IN, USA) were group-housed under conditions of constant photoperiod (12 h light, 12 h dark) with ad libitum access to sterilized food and water. All experimental procedures using mice were done in accordance with protocols approved by the Institutional Animal Care and Use Committee of The Ohio State University (US Office of Laboratory Animal Welfare, Assurance #A3261-01). Ectopic tumors were established in athymic nude mice by subcutaneous injection of PC-3 cells (1×10⁶ cells per mouse). The establishment and growth of tumors were monitored by direct measurement with calipers. Mice with established tumors (mean starting tumor volume ~50 mm³) were randomized to three treatment groups (n=7). Mice were treated once daily for 28 days by oral gavage with a) compound **1** at 50 mg kg⁻¹ body weight, b) compound **59** at 50 mg kg⁻¹ body weight, or c) vehicle (10% DMSO/0.5% methylcellulose/0.1% Tween 80 [v/v] in sterile water). Tumor burdens were determined weekly using calipers [tumor volume = (width)² × (length) × 0.52].

Statistical analysis: In vitro experiments were performed using 3–6 replicates in each group. All in vitro experiments were carried out at least twice on different occasions. Differences between group means of tumor burden were analyzed for statistical significance using two-sided Student *t* tests. Differences were considered significant at $p < 0.05$.

Abbreviations

ACC: acetyl-CoA carboxylase; AICAR: 5-aminoimidazole-4-carboxamide ribonucleotide; AMPK: adenosine monophosphate activated protein kinase; CBM: carbohydrate binding module; EMT: epithelial–mesenchymal transition; LKB1: liver kinase B1; MDM2: murine double minute 2; MTT: 3-(4,5-dimethylthiazol-2-yl)-2,5-diphenyl-2H-tetrazolium bromide; PTEN: phosphatase and tensin homologue.

Acknowledgements

This work was supported by the US National Institutes of Health grant R01CA112250 (C.S.C.) and a joint supervision fellowship from the Egyptian government (E.M.E.D.).

Keywords: AMPK • activators • antitumor agents • drug discovery • lead optimization

- [1] B. B. Kahn, T. Alquier, D. Carling, D. G. Hardie, *Cell Metab.* **2005**, *1*, 15–25.
- [2] Y. C. Long, J. R. Zierath, *J. Clin. Invest.* **2006**, *116*, 1776–1783.
- [3] C. T. Lim, B. Kola, M. Korbonits, *J. Mol. Endocrinol.* **2010**, *44*, 87–97.
- [4] D. G. Hardie, *Genes Dev.* **2011**, *25*, 1895–1908.
- [5] B. B. Zhang, G. Zhou, C. Li, *Cell Metab.* **2009**, *9*, 407–416.
- [6] D. G. Hardie, *Annu. Rev. Pharmacol. Toxicol.* **2007**, *47*, 185–210.
- [7] D. G. Hardie, *Cold Spring Harbor Symp. Quant. Biol.* **2011**, *76*, 155–164.
- [8] H. C. Chuang, C. C. Chou, S. K. Kulp, C. S. Chen, *Curr. Pharm. Des.* **2014**, *20*, 2607–2618.
- [9] A. Leone, E. Di Gennaro, F. Bruzzese, A. Avallone, A. Budillon, *Cancer Treat. Res.* **2014**, *159*, 355–376.
- [10] W. W. Wheaton, S. E. Weinberg, R. B. Hamanaka, S. Soberanes, L. B. Sullivan, E. Anso, A. Glasauer, E. Dufour, G. M. Mutlu, G. S. Budigner, N. S. Chandel, *Elife* **2014**, *3*, e02242.
- [11] K. H. Lee, E. C. Hsu, J. H. Guh, H. C. Yang, D. Wang, S. K. Kulp, C. L. Shapiro, C. S. Chen, *J. Biol. Chem.* **2011**, *286*, 39247–39258.
- [12] C. C. Chou, K. H. Lee, I. L. Lai, D. Wang, X. Mo, S. K. Kulp, C. L. Shapiro, C. S. Chen, *Cancer Res.* **2014**, *74*, 4783–4795.
- [13] D. B. Shackelford, R. J. Shaw, *Nat. Rev. Cancer* **2009**, *9*, 563–575.
- [14] F. Giordanetto, D. Karis, *Expert Opin. Ther. Pat.* **2012**, *22*, 1467–1477.
- [15] Z. Wang, J. Huo, L. Sun, Y. Wang, H. Jin, H. Yu, L. Zhang, L. Zhou, *Curr. Comput.-Aided Drug Des.* **2011**, *7*, 214–227.
- [16] S. Rana, E. C. Blowers, A. Natarajan, *J. Med. Chem.* **2015**, *58*, 2–29.
- [17] B. Cool, B. Zinker, W. Chiou, L. Kifle, N. Cao, M. Perham, R. Dickinson, A. Adler, G. Gagne, R. Iyengar, G. Zhao, K. Marsh, P. Kym, P. Jung, H. S. Camp, E. Frevert, *Cell Metab.* **2006**, *3*, 403–416.
- [18] T. Pang, Z. S. Zhang, M. Gu, B. Y. Qiu, L. F. Yu, P. R. Cao, W. Shao, M. B. Su, J. Y. Li, F. J. Nan, J. Li, *J. Biol. Chem.* **2008**, *283*, 16051–16060.
- [19] J. H. Guh, W. L. Chang, J. Yang, S. L. Lee, S. Wei, D. Wang, S. K. Kulp, C. S. Chen, *J. Med. Chem.* **2010**, *53*, 2552–2561.
- [20] L. F. Yu, Y. Y. Li, M. B. Su, M. Zhang, W. Zhang, L. N. Zhang, T. Pang, R. T. Zhang, B. Liu, J. Y. Li, J. Li, F. J. Nan, *ACS Med. Chem. Lett.* **2013**, *4*, 475–480.
- [21] B. C. Bookser, Q. Dang, T. S. Gibson, H. Jiang, D. M. Chung, J. Bao, J. Jiang, A. Kassick, A. Kekec, P. Lan, H. Lu, G. M. Makara, F. A. Romero, I. Sebhat, D. Wilson, D. Wodka (Merck Sharp & Dohme Corp., Metabasis Therapeutics Inc., Schering Corp.), Pat. Appl. No. CA 2741125 A1, **2010**.
- [22] B. Xiao, M. J. Sanders, D. Carmena, N. J. Bright, L. F. Haire, E. Underwood, B. R. Patel, R. B. Heath, P. A. Walker, S. Hallen, F. Giordanetto, S. R. Martin, D. Carling, S. J. Gambin, *Nat. Commun.* **2013**, *4*, 3017.
- [23] L. M. Lima, E. J. Barreiro, *Curr. Med. Chem.* **2005**, *12*, 23–49.
- [24] N. A. Meanwell, *J. Med. Chem.* **2011**, *54*, 2529–2591.
- [25] R. J. Dowling, M. Zakikhani, I. G. Fantus, M. Pollak, N. Sonenberg, *Cancer Res.* **2007**, *67*, 10804–10812.
- [26] J. B. Baell, L. Ferrins, H. Falk, G. Nikolakopoulos, *Aust. J. Chem.* **2013**, *66*, 1483–1494.
- [27] J. B. Baell, G. A. Holloway, *J. Med. Chem.* **2010**, *53*, 2719–2740.
- [28] J. Baell, M. A. Walters, *Nature* **2014**, *513*, 481–483.
- [29] E. F. Pettersen, T. D. Goddard, C. C. Huang, G. S. Couch, D. M. Greenblatt, E. C. Meng, T. E. Ferrin, *J. Comput. Chem.* **2004**, *25*, 1605–1612.

Received: August 15, 2015

Published online on September 9, 2015